
Article:
Ma, X.Y., Li, G. orcid.org/0000-0002-5956-4033, Zhu, Z.Q. et al. (2 more authors) (2018) Investigation on synchronous reluctance machines with different rotor topologies and winding configurations. IET Electric Power Applications, 12 (1). pp. 45-53. ISSN 1751-8660

https://doi.org/10.1049/iet-epa.2017.0199

Investigation on Synchronous Reluctance Machines with Different Rotor Topologies and Winding Configurations

X. Y. Ma, G. J. Li, Z. Q. Zhu, G. W. Jewell, J. E. Green

Department of Electronic and Electrical Engineering, University of Sheffield, Sheffield, S10 2TN, U.K.
g.li@sheffield.ac.uk.

Abstract: This paper investigates the influence of rotor topologies and winding configurations on the electromagnetic performance of 3-phase synchronous reluctance machines with different slot/pole number combinations, e.g. 12-slot/4-pole and 12-slot/8-pole. Transversally laminated synchronous reluctance rotors with both round flux barrier and angled flux barrier have been considered, as well as the doubly-salient rotor as that used in switched reluctance machines. Both concentrated and distributed winding configurations are accounted for, i.e., single layer and double layer conventional and mutually coupled windings, as well as fully-pitched winding. The machine performance in terms of *d*- and *q*-axis inductances, on-load torque, copper loss, and iron loss have been investigated using 2-D finite-element analysis. With appropriate rotor topology, 12-slot/4-pole and 12-slot/8-pole machines with fully-pitched and double layer mutually coupled windings can achieve similar torque capacity, which are higher than the machines with other winding configurations. In addition, the synchronous reluctance machine with round flux barrier can have lower iron loss than doubly salient reluctance machine under different working conditions. The prototypes of 12-slot/8-pole single layer and double layer, doubly salient synchronous reluctance machines have been built to validate the predictions in terms of inductances and torques.

Nomenclature

DSRM	Doubly Salient Reluctance Machine
SynRM	Synchronous Reluctance Machine
RFB	Round Flux Barrier
AFB	Angled Flux Barrier
DLC	Double Layer Conventional
DLMC	Double Layer Mutually Coupled
SLC	Single Layer Conventional
SLMC	Single Layer Mutually Coupled
FP	Fully-Pitched

1. Introduction

COMPARED with permanent magnet machines and induction machines, both the synchronous reluctance machines (SynRM) and the switched reluctance machines (SRMs) are becoming increasingly attractive in various applications ranging from domestic appliances to electrical vehicles and hybrid electrical vehicles (EVs and HEVs). This is mainly due to their magnet-free features and hence low cost, simple and robust rotor structures (without rotor conductors and hence no rotor copper losses), and hence very suitable for high speed and harsh environment applications [1]-[4]. In general, the SynRMs use standard 3-phase pulse width modulation (PWM) inverters while the SRMs require an

unconventional power-converter due to the square wave unipolar current supply (usually 120 degrees conduction for 3-phase SRMs) [1], [5]. This to some extent limits the wider industrial penetration of the SRMs. In order to employ the standard and off-the-shelf 3-phase inverter as that used in SynRMs so to reduce the system cost, in [5]-[7], the SRMs have been supplied with 3-phase sinewave currents, which are in effect short-pitched doubly salient reluctance machines (DSRMs).

Similar to the induction machines, the classic SynRMs often employ the distributed stator windings [8]. However, many permanent magnet machines and DSRMs adopt the fractional-slot concentrated windings due to their inherent advantages such as higher slot fill factor, shorter end-winding, smaller machine overall footprint, etc. [9]-[11]. When a fractional slot, double layer (DL) concentrated winding is applied to a 6-slot/4-pole (6/4) SynRM, it has been found that its torque density and efficiency as well as thermal characteristics can be effectively improved [12]. For the DSRMs, both the short-pitched (SP) concentrated windings and the FP distributed windings can be employed and this has been well investigated in literature [5], [13]. It has been found that the DSRM equipped with DL mutually coupled (DLMC) winding, which is also a SP winding, is less sensitive to magnetic saturation than the ones equipped with the DL conventional (DLC) windings and hence, produce higher average torque at high phase current [5]. However, the torque ripple coefficient of the DSRM equipped with the DLMC windings is relatively higher due to its nature of self- and mutual-inductances [14]. The FP distributed winding DSRM can generate lower torque ripple but its long end-winding will result in higher copper loss for a given phase current. In order to take advantage of both the FP distributed windings (higher torque capability) and the SP concentrated windings (shorter end-winding), single layer (SL) concentrated windings (SLC and SLMC) DSRMs have been proposed in [5]. They can have higher torque capability than the DL concentrated windings (DLC and DLMC) counterparts but lower copper loss than that of the FP distributed windings.

Although the rotor of the DSRM is simpler and easier for manufacturing than that of the SynRM, the doubly salient (DS) rotor structure will result in high levels of acoustic noise and vibration [15]-[16]. In contrast, most SynRMs have non-salient rotors with various topologies in order to increase the saliency ratio and also the difference between *d*- and *q*-axis inductances, and hence to increase the torque capability [1], [2]. It is well established in literature that the SynRMs are generally designed with transversally laminated rotor [17], [12]. Although the axially laminated rotor has advantages such as increased saliency ratio, hence improved power density and power factor [18]-[19], it is very complex for industrial manufacturing. Therefore, the transversally laminated rotor has been selected for investigation in this paper. By way of example, rotors with 4 poles are illustrated and they generally have two shapes, e.g. round flux barrier (RFB) and angled flux barrier (AFB) [17], [20]-[21]. The latter is also used for some permanent magnet assisted SynRMs as shown in [22]-[23]. It has been found in [18] that with the distributed windings, the three flux barrier layers SynRM can produce similar average

torque but lower torque ripple than other numbers of flux barrier layer. In addition, the influence of slot numbers on the average torque is very minor but lower torque ripple can be produced with higher slot numbers. Hence, the three-layer flux-barrier in the rotor will be adopted for the 12/4 and 12/8 machines in this paper.

For clarity, a diagram including rotor topologies, slot/pole number combinations and winding configurations for all the investigated reluctance machines in this paper is shown in Fig. 1. The three rotor topologies: SynRM-RFBs, SynRM-AFBs and DSRM will be investigated for both the 12/4 and 12/8 slot/pole number combinations. In addition, the DL and SL conventional windings (DLC and SLC), the DL and SL mutually-coupled windings (DLMC and SLMC), as well as the FP winding will be employed and are illustrated in Fig. 1. By way of example, the *d*- and *q*-axis inductances and power factors will be investigated on 12/8 machines with different windings and rotor topologies. For the performance investigations throughout this paper, appropriate rotor structures will be identified based on torque comparison at both low and high current levels for both the 12/4 and 12/8 machines. Then, comparison in terms of average torque, torque ripple, copper loss and iron loss will be carried out by 2-D finite element analysis (FEA) between different slot/pole number combinations and winding configurations for the machines with appropriate rotor topologies.

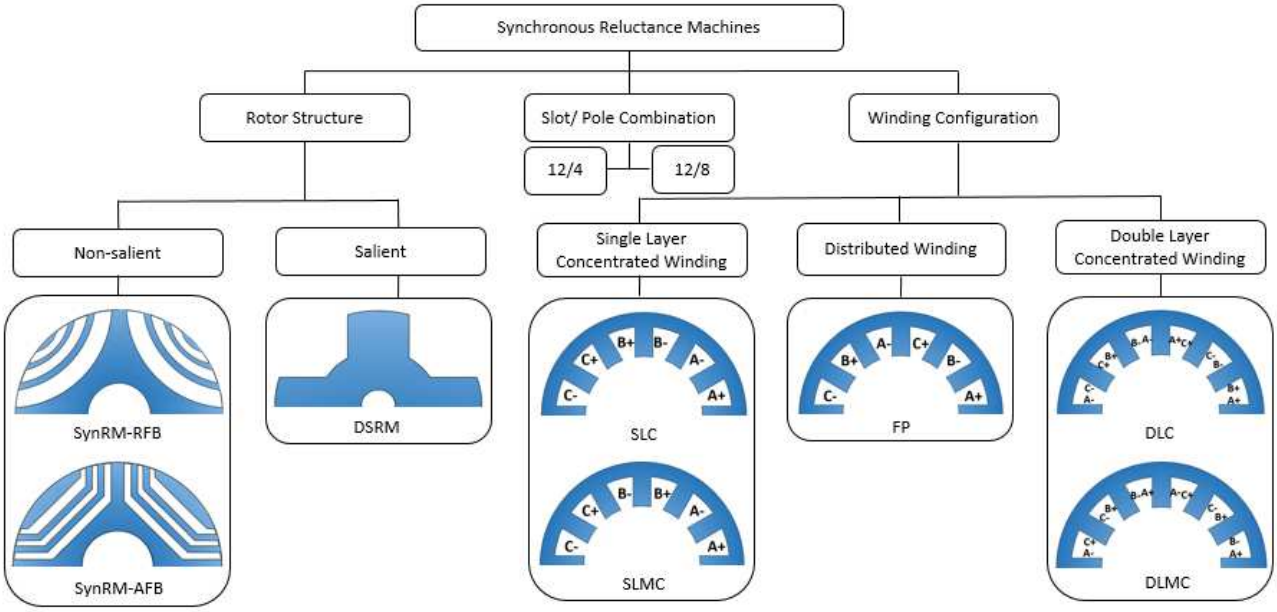

Fig. 1. *Investigated reluctance machines in this paper with different winding configurations and rotor topologies.*

2. Features of Reluctance Machines

2.1. Different Rotor Topologies and Winding Configurations

For fairer comparison throughout this paper, machines with different windings and rotor topologies have been optimized separately, and the optimization objective is to achieve the highest torque for constant copper loss (Only dc losses have been considered, the end-winding has also been included in copper loss calculations). It is worth mentioning that for the concentrated windings, only the

SL windings have been selected for optimization mainly because they can generally produce higher average torque than their DL counterparts. Hence, the dimensions of stator core are kept the same for all the winding configurations. However, the stator core has been optimized separately for machines with different rotor structure. The main dimensions of all investigated machines are kept the same as shown in Table 1. The rib width is 0.3mm for all SynRMs. However, the stator inner radii for 12/8 SynRM-RFB, SynRM-AFB, and DSRM are optimized as 27mm, 27mm and 28.4mm, and the shaft outer radii are 13mm, 9mm and 11.6mm, respectively.

Table 1 General dimensions and design parameters of reluctance machines

Stator slot number	12	Active length (mm)	60
Rotor pole number	4/8	Number of turns per phase	132
Stator outer radius (mm)	45	Slot area (mm^2)	116
Air gap length (mm)	0.5	Current density (A_{rms}/mm^2)	5.68

As mentioned previously, the SynRMs with three-layer flux-barrier in the rotor have been selected for investigation in this paper. By way of example, the flux line distribution of the optimized 12/8 SynRMs with both round and angled flux-barrier rotors and different winding configurations, as well as the 12/8 DSRM are shown in Fig. 2. Phase A is supplied with a 10A dc current and the rotor pole is aligned with the phase A. It can be found that there is no flux through the phase B and the phase C for the conventional concentrated windings as shown in Fig. 2a. However, the mutual fluxes present in both the MC winding (Fig. 2b) and the FP windings (Fig. 2c).

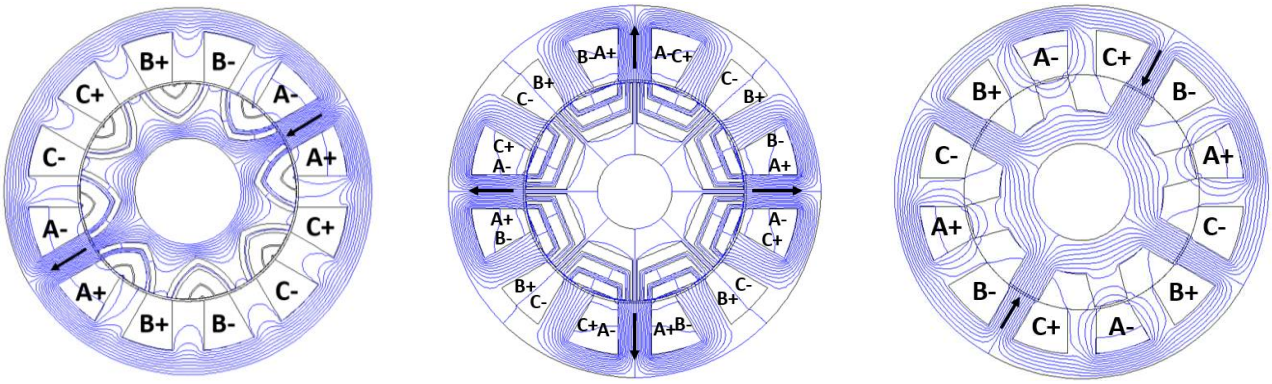

a *b* *c*

Fig. 2. *Flux line distributions of 12/8 reluctance machines with different rotor topologies and winding configurations. The rotor pole is at the aligned position with the phase A, which is supplied with a 10A current.*
a SynRM with RFBs and SLC winding
b SynRM with AFBs and DLMC winding
c DSRM with FP winding

The material M330-35A is used for the prototype machines, which has a yield stress of 300MPa and a material density of $7650kg/m^3$. By using 2D FEA, the maximum speed of 19000 rpm and mechanical stress of 295MPa for the 8-pole SynRM rotor with AFBs have been obtained. However, 8-pole SynRM rotor with RFBs and DSRM rotor can achieve much higher speed, i.e. 26000 rpm and

47000 rpm, respectively. Fig. 3 shows the comparison of mechanical stress σ and radial displacement u between different rotors at 19000 rpm. It is found that at this speed, the displacements of the rotor into air-gap are lower than 1.84% of the air gap length (0.5mm). This means that the rotor will not rub the stator inner surface at this operating speed.

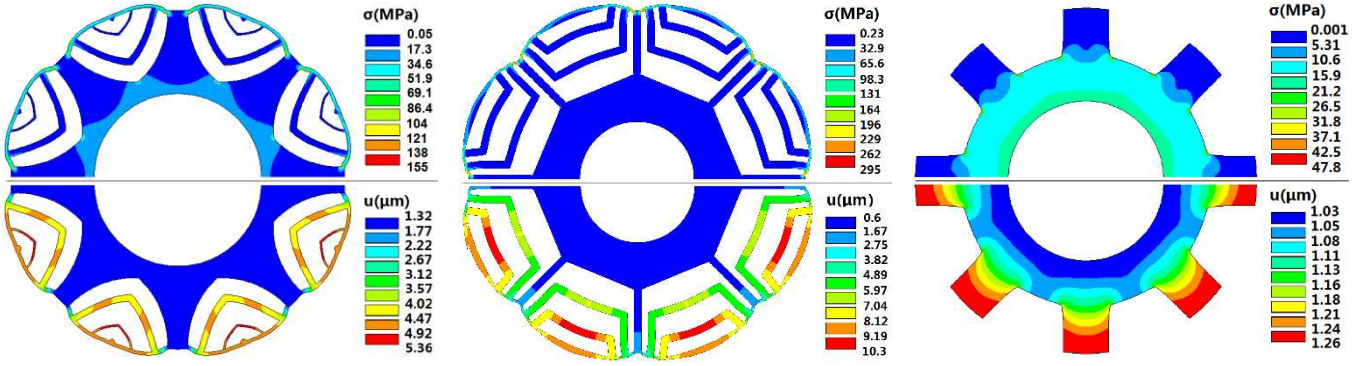

a *b* *c*

Fig. 3. *Mechanical stress σ and radial displacement u comparison between different 8-pole rotors at 19000 rpm.*
a SynRM with RFBs
b SynRM with AFBs
c DSRM

Accordingly, coil magnetic polarities for different winding configurations are illustrated in Table 2. It can be found that the coil magnetic polarities of the SLC and SLMC machines are similar to those of the DLC and DLMC machines, respectively. However, compared with the DL machines, the SL machines have half number of coils per phase under the condition that the number of turns per phase (132) is the same for both the DL and SL machines. Similar to the SL windings, the FP windings have only two coils per phase but each coil spans three stator slot pitches due to the distributed winding configuration as shown in Fig. 1. This will lead to longer end-winding, hence potentially higher copper loss than other winding configurations for the same phase RMS current.

Table 2 Coil magnetic polarities of reluctance machines with different winding configurations

Winding configurations			Coil magnetic polarities
Concentrated winding	SL winding	SLC	NSNSNS
		SLMC	NNNNNN
	DL winding	DLC	SNSNSNSNSNSN
		DLMC	SSSSSSSSSSS
Distributed winding	FP winding	FP	NSNSNS

2.2. Influence of Rotor Topologies and Winding Configurations on d- and q-Axis Inductances and Power Factors

Since the DSRMs are supplied with 3-phase sinewave currents and in effect become SynRMs but with salient rotors, the phasor diagram of the SynRMs can be applicable to the DSRMs as well. Accordingly, accounting for the cross-couplings, the d- and q-axis inductances L_d and L_q are described by

$$L_d(i_d, i_q) = \frac{\psi_d(i_d, i_q)}{i_d} \quad (1)$$

$$L_q(i_d, i_q) = \frac{\psi_q(i_d, i_q)}{i_q} \quad (2)$$

where ψ_d and ψ_q are the d- and q-axis stator flux linkages, i_d and i_q are the d- and q-axis stator currents, respectively. By way of example, the 12/8 machines have been selected to investigate the influence of rotor topologies and winding configurations on the d- and q-axis inductances. Table 3 compares L_d and L_q of the 12/8 machine topologies with different rotor topologies and winding configurations. It can be found that the machines with the FP winding has the highest L_d and L_q at $10A_{rms}$ than others, regardless of rotor topologies. This will become an important factor that limits the constant power speed range. Additionally, the SL winding machines have higher L_d and L_q than their DL counterparts. The saliency ratio ($\zeta = \frac{L_d}{L_q}$) in Table 4 shows that the machines with the DLMC winding have the highest ζ, regardless of the rotor structures. Therefore, it can be predicted that the 12/8 machines with the DLMC winding could have better performance than others due to their highest saliency ratio. Furthermore, the power factors (see Table 4) can be obtained according to the phasor diagram of synchronous reluctance machines. It can be found that the SynRM-RFB can have the highest saliency ratio and power factors, regardless of winding configurations. Moreover, the power factors of the machines with DL windings are higher than that of the machines with SL windings. The machines with FP windings have the lowest power factors.

Table 3 Comparison of d- and q-axis inductances between different 12/8 machines at $\mathbf{10}\boldsymbol{A_{rms}}$ ($\boldsymbol{I_d = I_q}$)

	$\boldsymbol{L_d}$ (mH)			$\boldsymbol{L_q}$(mH)		
	SynRM-RFB	SynRM-AFB	DSRM	SynRM-RFB	SynRM-AFB	DSRM
SLC	6.9	7.3	7.7	3.9	4.5	4.7
SLMC	7.1	7.7	9.0	3.9	4.5	4.9
FP	11.9	9.9	14.1	7.8	8.7	8.4
DLC	3.5	3.2	4.8	2.4	2.8	2.7
DLMC	4.4	5.4	5.0	2.1	2.6	2.6

Table 4 Comparison of saliency ratio $\frac{\boldsymbol{L_d}}{\boldsymbol{L_q}}$ and power factors for different 12/8 machines at $\mathbf{10}\boldsymbol{A_{rms}}$ ($\boldsymbol{I_d = I_q}$)

	SynRM-RFB		SynRM-AFB		DSRM	
	L_d/L_q	Power Factor	L_d/L_q	Power Factor	L_d/L_q	Power Factor
SLC	1.787	0.676	1.639	0.638	1.635	0.621
SLMC	1.847	0.679	1.713	0.637	1.834	0.620
FP	1.523	0.576	1.135	0.508	1.680	0.567
DLC	1.459	0.778	1.122	0.741	1.787	0.745
DLMC	2.106	0.796	2.096	0.752	1.895	0.750

It is established that the electromagnetic torque performance can be determined by the difference between L_d and L_q. Hence, $(L_d - L_q)$ has been calculated with different winding configurations as

shown in Fig. 4. Also, the $(\frac{L_d}{L_q} - 1)$ of DSRMs has been shown in Fig. 4d. It is apparent that at low current, the highest $(L_d - L_q)$ of the SynRM-RFB and the DSRM are achieved by using the FP winding. However, for the SynRM-AFB, this can be obtained by using the SLMC winding. Therefore, at low current, the 12/8 FP-SynRM RFB and FP-DSRM can be predicted to produce higher torque than other 12/8 SynRM-RFBs and DSRMs, respectively. However, at high current, the DLMC winding produces the highest $(L_d - L_q)$, regardless of rotor topologies. Hence, it could be predicted that all the three 12/8 machine topologies can achieve their best torque performances at high current levels when the DLMC winding configuration is employed. Moreover, the 12/8 DLMC-DSRM could potentially generate higher torque than the 12/8 DLMC-SynRMs due to slightly higher $(L_d - L_q)$.

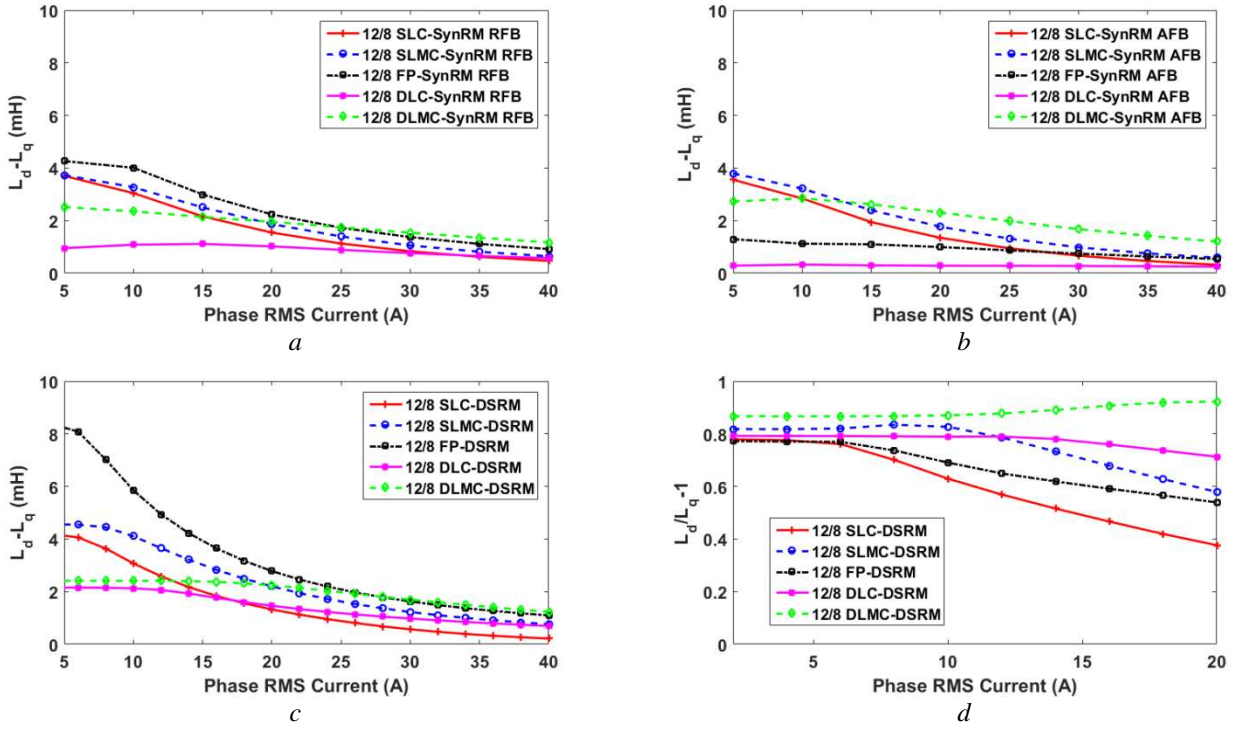

Fig. 4. *Comparison of* $(L_d - L_q)$ *and* $(\frac{L_d}{L_q} - 1)$ *against phase RMS current between 12/8 reluctance machines. The machines are supplied with 3-phase sinewave currents with* $I_d = I_q$.

a $(L_d - L_q)$ of SynRM with RFBs
b $(L_d - L_q)$ of SynRM with AFBs
c $(L_d - L_q)$ of DSRM
d $(\frac{L_d}{L_q} - 1)$ of DSRM

3. Torque Performances for Different Windings, Rotor Topologies and Pole Numbers

3.1. Influence of Rotor Topologies on Torque Performances for both the 12/4 and 12/8 Machines

According to the d- and q-axis inductances, the electromagnetic torque of a 3-phase reluctance machine can be calculated by

$$T = \frac{3}{2} \times p(L_d - L_q) I_d I_q = \frac{3}{4} \times p(L_d - L_q) {I_s}^2 \sin\alpha \tag{3}$$

where p is the pole pair number, α is the current phase angle, and I_s is the phase peak current, respectively. It is apparent that the maximum average torque will be obtained at $\alpha = 45°$ ($I_d = I_q$) without considering magnetic saturation [1], [20]. For completeness, average torques at different current levels of all the 12/4 and 12/8 machines have been obtained by 2D-FEA, as shown in Fig. 5. The torque ripple coefficient is calculated by $T_{ripple} = \frac{T_{max} - T_{min}}{T_{av}} \times 100\%$, where T_{max}, T_{min} and T_{av} are the maximum, minimum and average torques over one electrical cycle. It is worth noting that with different pole numbers and winding configurations, the reluctance will be different due to different winding factors and airgap permeances. Hence, their influence on torque performances will be investigated separately in the following sections.

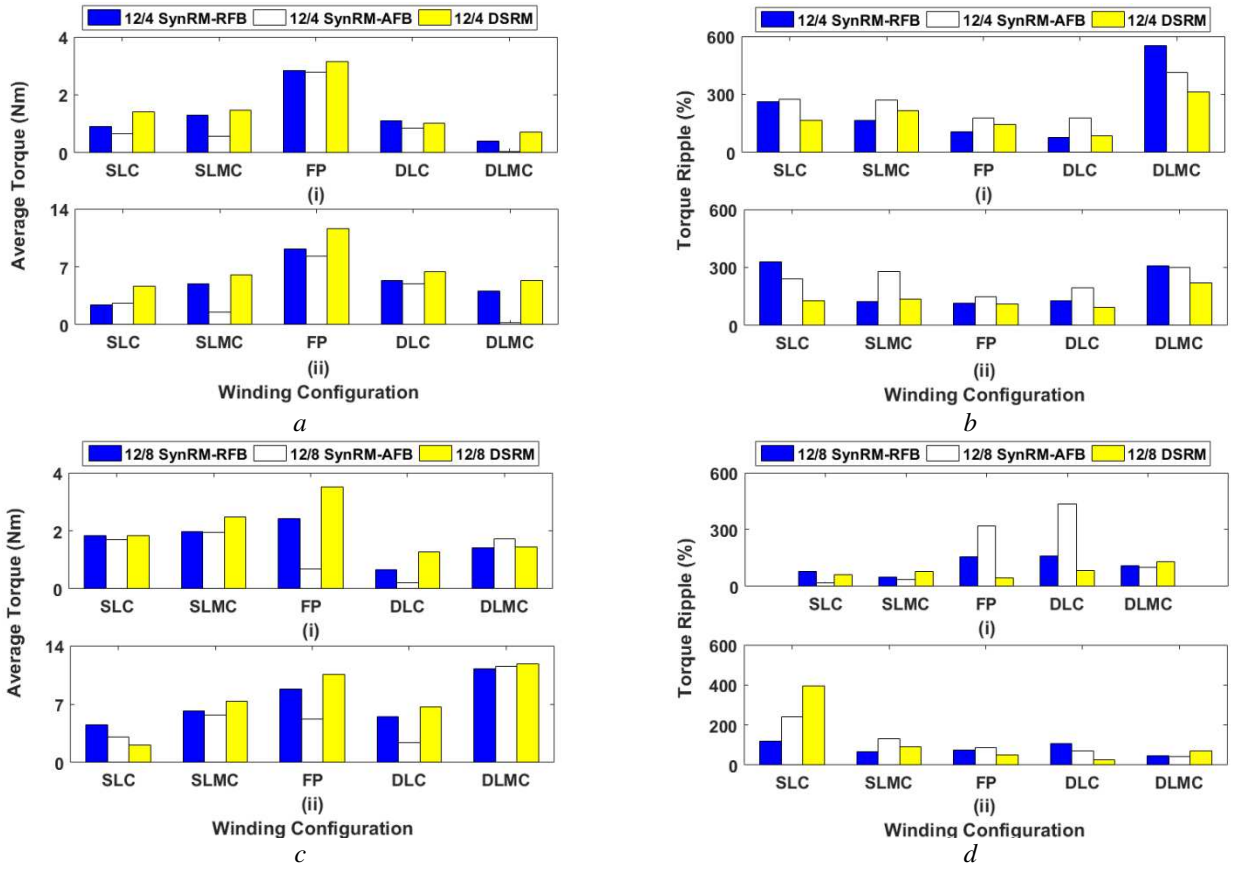

Fig. 5. *Torque performance of the 12/4 and 12/8 SynRMs and DSRMs with different winding configurations at (i) 10 Arms and (ii) 40 Arms.*
a Average torque of 12/4 machines
b Torque ripple coefficient 12/4 machines
c Average torque of 12/8 machines
d Torque ripple coefficient of 12/8 machines

It can be found that for the SynRMs, the RFB rotor can produce higher average torque than the AFB rotor due to 20% higher average ratio of flux barrier thickness to the combined thickness of lamination and flux barrier, hence higher $\frac{L_d}{L_q}$ [1] . This is true for almost all winding configurations and for both low and high current levels (except the 12/4 SLC winding at high current and the 12/8 DLMC winding). However, the 12/4 and 12/8 DSRMs can produce similar or even higher average torque than

the SynRMs at both low and high current levels, regardless of winding configurations. The SynRMs with AFB rotor produce higher torque ripple than the DSRMs and the SynRMs with RFB rotor for most winding configurations. However, with similar average torque, the AFB rotor can produce lower torque ripple at 12% for the 12/8 SLC winding at low current. Accordingly, the appropriate rotor topologies to obtain the maximum average torque for both the 12/4 and 12/8 machines with different winding configurations have been summarized in Table 5. For clarity, only the most appropriate rotor topologies have been selected for further investigations.

Table 5 Appropriate rotor topologies to obtain the maximum average torque

Slot/pole combinations	Winding configurations				
	SLC	SLMC	FP	DLC	DLMC
12/4	DSRM	DSRM	DSRM	SynRM-RFB &DSRM	DSRM
12/8	SynRM-RFB &DSRM	DSRM	DSRM	DSRM	SynRM-AFB &DSRM

3.2. Influence of Slot/Pole Number Combinations on Torque Performance with Appropriate Rotor Topologies

With the appropriate rotor topologies such as the ones shown in Table 5, the influence of slot/pole number combinations on torque-speed characteristics under $\mathrm{I_{max}} = 14.14\mathrm{A}$ and $\mathrm{V_{dc}} = 100\mathrm{V}$ is shown in Fig. 6.

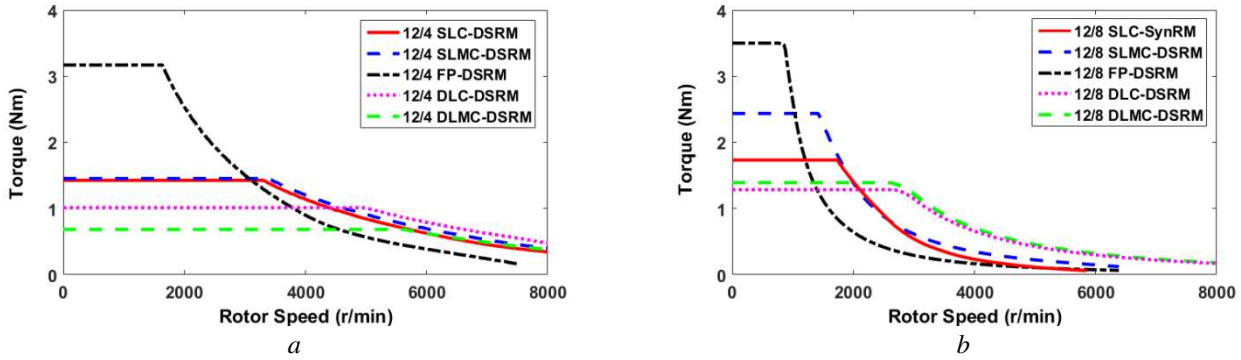

Fig. 6. *Torque-speed curves between 12/4 and 12/8 machines with different windings.* $I_{max} = 14.14A$ and $V_{dc} = 100V$.
a 12/4 machines
b 12/8 machines

It can be found that both the 12/4 and 12/8 machines with the FP windings and the doubly salient rotors can achieve their best initial torques at $10A_{rms}$. However, the 12/4 machines can have wider constant torque range than the 12/8 machines. In addition, it is also found that the DL machines can have higher base speed than other machines. However, the FP machines have the highest initial torque but the lowest base speed under the limit of $I_{max} = 14.14\mathrm{A}$ and $V_{dc} = 100\mathrm{V}$. It is worth mentioning that the 4-pole machines would produce less iron losses due to lower electrical frequency than the 8-pole machines. This will be investigated in the following section.

4. Influence of Machine Topologies on Copper Loss and Iron Loss

It is well-established that the copper loss (proportional to current squared) could be the dominant loss for high torque low speed applications, while the iron loss could be the dominant loss for high speed applications, where the iron losses are determined by the iron core flux density and also the electrical frequency. Therefore, the aforementioned influence of winding and rotor topologies on torque performance will also be reflected into the machine losses.

4.1. Copper Loss

Due to different end-windings, the winding configurations will have significant influence on the copper loss characteristics. However, if phase current is unchanged then the different rotor pole numbers and rotor topologies will have no influence on copper loss for the same sized machines. Due to longer end-windings, the FP machines will generally produce higher copper loss than other machines, regardless of current levels. At $10A_{rms}$, the copper loss of the FP (246W) can be around 1.5 times higher than that of the SL (173W) and DL (154W) winding machines.

Although the FP machines generate higher copper loss than the SL and DL winding machines, the average torque against copper loss characteristics could be more important for investigation because the FP machines could generate higher average torque as well, as investigated previously. With appropriate rotor topologies, both average torque and torque ripple against copper loss for machines with different winding configurations have been obtained, as shown in Fig. 7. At lower torque level, e.g. 4Nm, both the 12/4 and 12/8 FP-DSRM will produce lower copper loss. At high torque level, e.g. 6Nm, the 12/4 machine with the FP winding still have the best torque against copper loss performance than others. However, for the 12/8 machines, the copper loss of the DLMC winding is about one-half of the 12/8 FP winding machine at 10Nm. Moreover, the 12/8 DLMC machine exhibits even higher average torque at high currents. This is due to the fact that the machines with the DLMC windings have lower mmf concentration in the stator yoke, hence are less sensitive to the magnetic saturation. Nevertheless, they exhibit higher torque ripple than the FP winding machines due to their nature of self- and mutual-inductances as mentioned previously. It is also found that with appropriate winding configurations, the torque capability of the 12/4 machines is similar to that of the 12/8 machines. Overall, it can be concluded that with the FP windings, both the 12/4 and 12/8 machines can have better torque against copper loss characteristics without heavy magnetic saturation. However, the 12/8 DLMC machines can have better performance at high current levels (high copper loss).

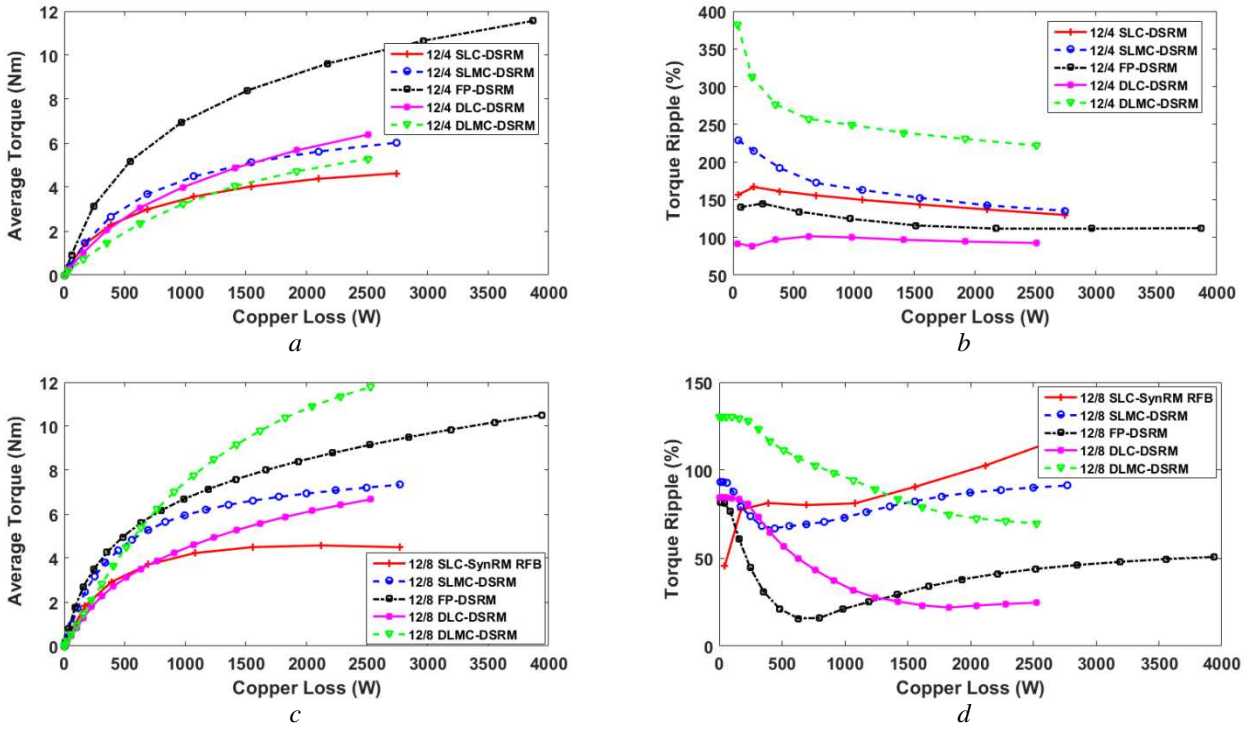

Fig. 7. *Influence of slot/pole number combinations and winding configurations on average torque and torque ripple against copper loss.*

a Average torque against copper loss of 12/4 machines

b Torque ripple against copper loss of 12/4 machines

c Average torque against copper loss of 12/8 machines

d Torque ripple against copper loss of 12/8 machines

4.2. Iron Loss

Different from copper loss, the iron loss can be influenced not only by the winding configurations, but also by the slot/pole number combinations and rotor topologies. Considering the torque performance, the FP and SLMC windings are selected for the 12/4 machines, whilst the FP and DLMC windings are selected for the 12/8 machines. Moreover, both the DSRM and SynRM rotors are selected for iron loss investigation. The iron loss density over one electrical cycle is comprised of hysteresis loss and eddy-current loss, which can be calculated as [24]:

$$p_{iron}\ (W/m^3) = f\left(k_{h1}\Delta B_{pp} + k_{h2}\Delta {B_{pp}}^2\right) + k_e f \int_0^{1/f} \left(\frac{\partial B}{\partial t}\right)^2 dt \tag{4}$$

Where f is the stator or rotor flux density frequency, B_{pp} is the peak-to-peak flux density. For the silicon iron cores considered in these machines, the hysteresis loss coefficients k_{h1} and k_{h2} are $5A/m$ and $40A/m$, and the eddy current loss coefficient k_e is $0.022\ Am/V$.

The total iron loss is obtained by the summation of the iron losses calculated in every individual FE mesh element in both the stator and the rotor. According to (4), it is necessary to investigate the radial and tangential flux densities (B_r and B_t) frequencies and their variations for both the stator and the rotor, as shown in Table 6. It is worth noting that the rotor topology does not have any influence on the flux density frequencies.

Table 6 Flux density frequencies of the stator and the rotor

Slot/pole combination	Winding configuration	Stator B_r/B_t frequency (Hz)	Rotor B_r/B_t frequency (Hz)
12/4	FP	13.3	80
	SLMC	13.3	40
12/8	FP	26.6	40
	DLMC	26.6	80

It can be found that the stator flux density frequency is only influenced by the slot/pole number combination and it is equal to $p\Omega/60$, where Ω is the mechanical rotor speed, and p is the pole-pair number. This means that the stator flux density has 1 period in every electrical cycle. Nevertheless, the rotor flux density will present different frequencies due to different winding configurations and rotor pole numbers.

By way of example, the 12/8 FP and 12/8 DLMC machines have been shown in Table 7 for investigation on the stator and rotor iron losses at 10 A_{rms}, 400 rpm. It can be found that, with the same stator and rotor flux density frequencies, the SynRM-AFB generates higher stator and rotor iron loss than the DSRM with 12/8 DLMC windings due to higher variations in B_r and B_t. However, the SynRM-RFB will generate lower stator and rotor iron loss than the DSRM with 12/8 FP windings due to lower variations in B_r and B_t.

Table 7 Iron loss of 12/8 machines at $\mathbf{10A_{rms}}$ and 400 rpm

Machines	Iron loss (W)		
	Stator	Rotor	total
12/8 FP-SynRM RFB	1.79	1.86	3.65
12/8 FP-DSRM	2.24	2.45	4.69
12/8 DLMC-SynRM AFB	0.59	1.03	1.63
12/8 DLMC-DSRM	0.57	0.24	0.81

According to the torque capability, two rotor topologies have been selected for the 12/4 and 12/8 machines with appropriate winding configurations. For completeness, the influences of phase RMS current and speed on total iron loss have been calculated, as shown in Fig. 8. It can be found that for the 12/4 machines, the SynRM-RFB with FP winding can produce the lowest iron losses for the full speed and current ranges. However, for the 12/8 machines, the DSRM with DLMC winding produces the lowest iron losses for the full speed and current ranges. Moreover, it is found that the 12/8 machines have higher iron loss than the 12/4 machines with the same rotor topologies and windings at variable current levels and speeds, as expected.

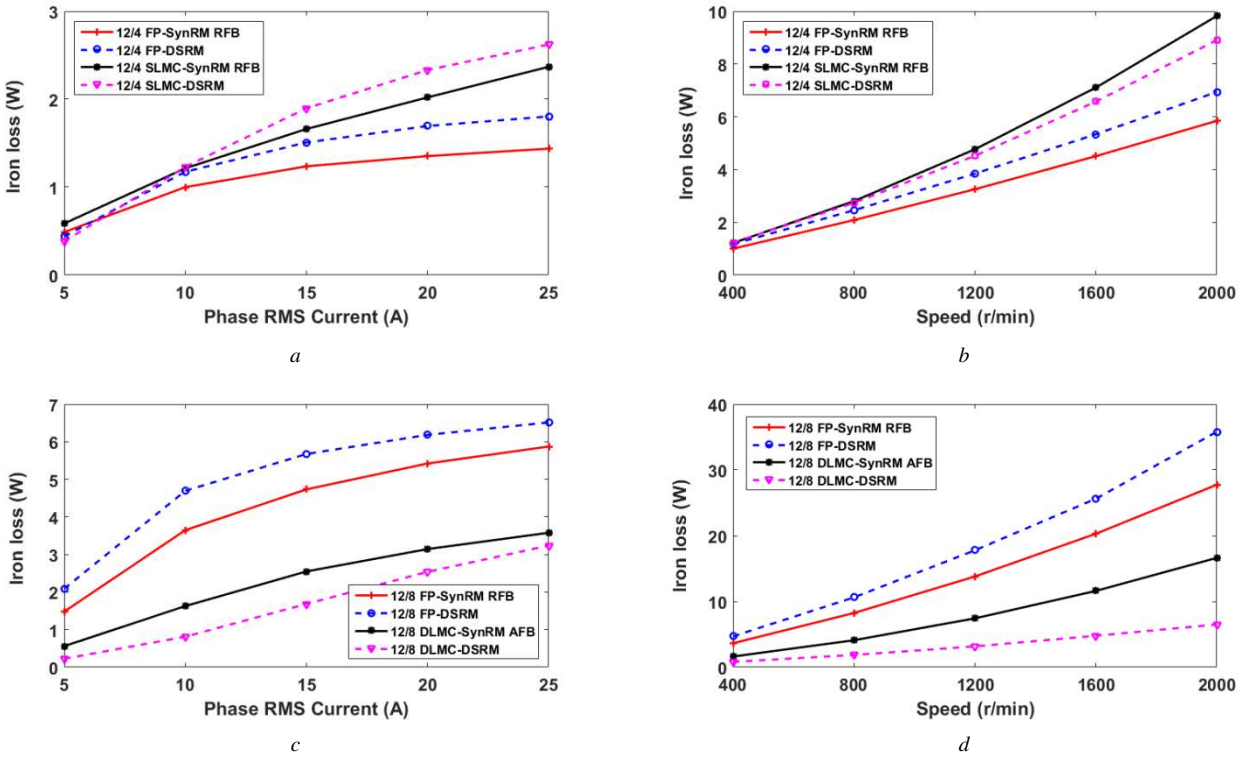

Fig. 8. *Iron loss of selected 12/4 and 12/8 machines under different operating conditions.*
a 12/4 machines at 400 rpm with increasing phase RMS current
b 12/4 machines at 10Arms with increasing speed
c 12/8 machines at 400 rpm with increasing phase RMS current
d 12/8 machines at 10Arms with increasing speed

5. Experimental Validation

In order to validate the predictions, both the 12/8 SL-DSRMs and the 12/8 DL-DSRMs that have been built in [5] are employed in this paper, and the inductances and static torques have been measured as detailed in the following sections. The FP winding has not been built due to its significantly longer end-winding than other winding configurations, leading to higher copper loss. In addition, it has relatively lower power factor.

The self- and mutual-inductances of the 12/8 DSRMs with different windings are measured against rotor positions at 1A dc current as shown in Fig. 9. The measured phase resistances of the SL- and DL-DSRMs are 1.48Ω and 1.32 Ω, respectively. The method of static torque measurement in [25] has been adopted for undertaking the torque measurements in this paper. In order to measure the static torque, three phases of the DSRMs are supplied with dc currents such as $I_A = I$, $I_B = I_C = -1/2I$, where I is variable and controllable by the power supply. The static torques against rotor positions for variable currents have been measured as shown in Fig. 10. It can be found that the measured results are in good agreement with the predicted results.

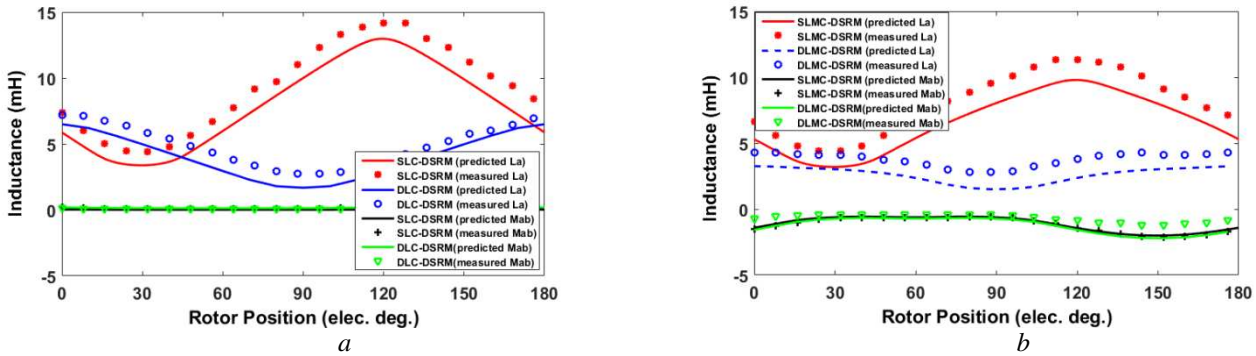

a *b*

Fig. 9. *Measurement of self- and mutual-inductances of 12/8 DSRMs with different windings at 1A dc current.*
a 12/8 conventional winding DSRMs
b 12/8 mutually-coupled winding DSRMs

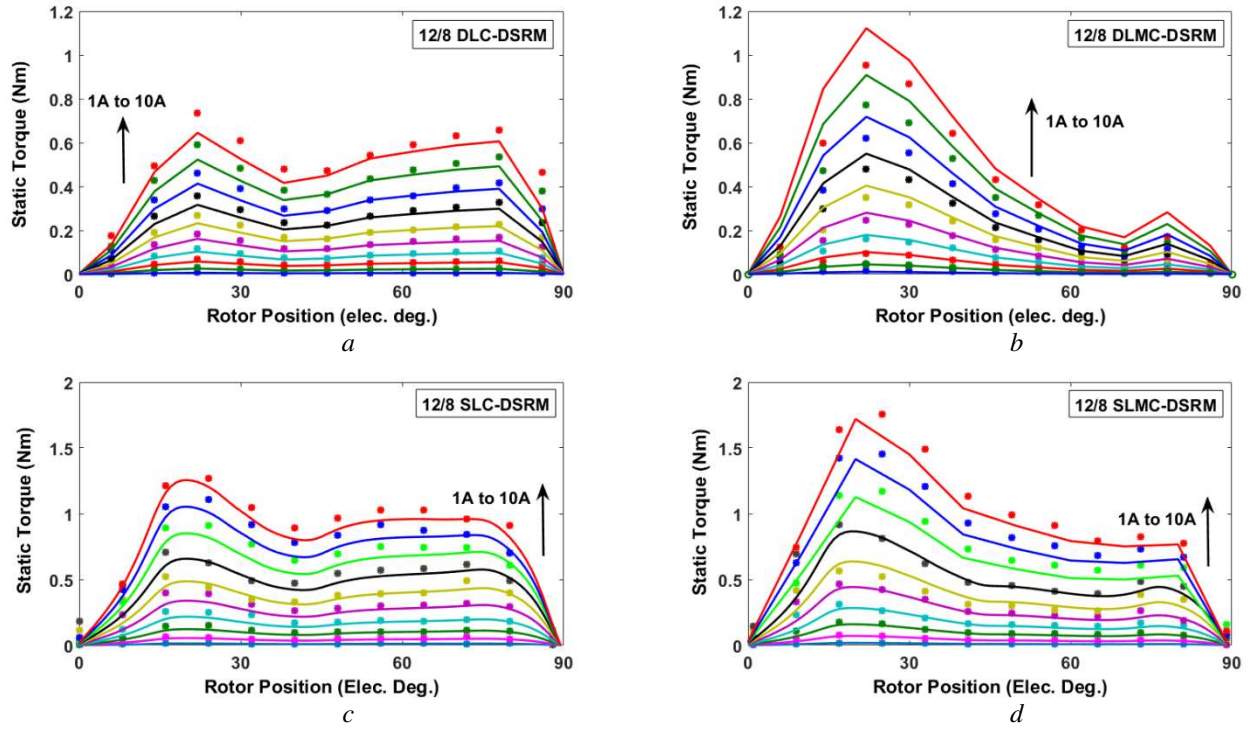

a *b*

c *d*

Fig. 10. *Static torque against rotor position for variable currents (solid line: predicted results, dot: measured results)*
a 12/8 DLC-DSRM
b 12/8 DLMC-DSRM
c 12/8 SLC-DSRM
d 12/8 SLMC-DSRM

Furthermore, the machine efficiency has been obtained for both the 12/8 SL- and DL-DSRMs as shown in Table 8 where the dc link voltage is 18V and the maximum phase peak current is 6A, which is limited by the load-torque capacity of the used dc machine. The low efficiency is mainly due to the fact that for the prototype machines, smaller copper wires have been used to ease the winding process, leading to smaller slot filling factor and higher copper loss. The difference between predicted and measured results is mainly because the end-winding effect has not been taken into account in the 2-D FEA. In addition, the torque-sensor accuracy and measuring error can be the other factors that contribute to this discrepancy.

Table 8 Machine efficiency (%) of 12/8 SL- and DL-DSRMs at $\mathbf{10A_{rms}}$ and 400 rpm

Speed(rpm)	DLC-DSRM		DLMC-DSRM		SLC-DSRM		SLMC-DSRM	
	Predicted	Measured	Predicted	Measured	Predicted	Measured	Predicted	Measured
350	21.24	16.86	22.37	17.97	31.71	24.67	32	26.2
400	23.56	20.30	24.77	21.83	34.67	28.31	34.98	30.56
450	25.74	22.34	27.03	24.55	35.89	27.19	36.73	29.85
500	27.81	23.43	29.16	25.57	37.36	30.61	37.22	30.84
550	29.76	24.24	31.17	25.64	39.35	31.02	39.18	33.83
600	31.61	26.9	33.06	27.37	41.11	--	41.36	--

6. Conclusion

Three rotor topologies (SynRM-RFB, SynRM-AFB, and DSRM), five winding configurations (SLC, SLMC, FP, DLC, DLMC) and two slot/pole number combinations (12/4 and 12/8) are employed for investigation on the synchronous reluctance machines. By way of examples, the 12/8 SynRM-RFB can produce the highest power factors regardless of winding configurations. In addition, the power factors of DL windings are higher than both the SL and FP windings. The appropriate rotor topologies have been identified for each winding configuration and slot/pole number combination, according to the torque performance at different current levels. With appropriate rotor topology, the influence of slot/pole number combinations on average torque and torque ripple for different phase currents have been investigated. It has been found that the 12/4 and 12/8 machines have similar torque capability (12Nm at 40Arms) when the appropriate winding configurations are employed. By way of example, the FP winding is the most appropriate winding configuration for the 12/4 machines, while the DLMC winding is the best for the 12/8 machines.

Regarding the copper loss, the FP winding presents the best average torque against copper loss characteristics at low current for both the 12/4 and 12/8 machines. However, the 12/8 machines with the DLMC winding achieve better average torque against copper loss at high current due to their shorter end-windings. The investigation on iron loss shows that lower iron loss can be achieved by the SynRM-RFBs rotor topology when compared to the DSRMs. Moreover, the FP and DLMC windings can produce lower iron loss than other windings for the 12/4 and 12/8 machines, respectively.

7. Reference

[1] Staton D. A., Miller T. J. E. , Wood S. E., 'Maximising the saliency ratio of the synchronous reluctance motor', Proc. Inst. Elect. Eng. -Elect. Power Appl., 1993, **140**, (4), pp. 249-259.

[2] Matsuo T. , Lipo T. A., 'Rotor design optimization of synchronous reluctance machine', IEEE Trans. Energy Convers., 1994, **9**, (2), pp. 359-365.

[3] Miller T. J. E., 'Optimal design of switched reluctance motors', IEEE Trans. Ind. Electron., 2002, **49**, (1), pp. 15-27.

[4] Lipo T. A., "Synchronous reluctance machines- a viable alternative for AC drives," presented at the Proc. Wisconsin Elect. Mach. Power Electron. Consortium, Madison, USA, 1991.

[5] Ma X. Y., Li G. J., Jewell G. W., Zhu Z. Q. , Zhan H. L., 'Performance comparison of doubly salient reluctance machine topologies supplied by sinewave currents', IEEE Trans. Ind. Electron., 2016, **63**, (7), pp. 4086-4096.

[6] Liang X., Li G., Ojeda J., Gabsi M. , Ren Z., 'Comparative study of classical and mutually coupled switched reluctance motors using multiphysics finite-element modeling', IEEE Trans. Ind. Electron., 2014, **61**, (9), pp. 5066-5074.
[7] Ojeda X., Mininger X., Gabsi M. , Lecrivain M., 'Sinusoidal feeding for switched reluctance machine: application to vibration damping', ICEM, 2008, pp. 1-4.
[8] Moghaddam R. R. , Gyllensten F., 'Novel high-performance SynRM designmethod: an easy approach for a complicated rotor topology', IEEE Trans. Ind. Electron., 2014, **61**, (9), pp. 5058-5065.
[9] Reddy P. B., El-Refaie A. M., Huh K. K., Tangudu J. K. , Jahns T. M., 'Comparison of interior and surface PM machines equipped with fractional-slot concentrated windings for hybrid traction applications', IEEE Trans. Energy Convers., 2012, **27**, (3), pp. 593-602.
[10] El-Refaie A. M., Jahns T. M. , Novotny D. W., 'Analysis of surface permanent magnet machines with fractional-slot concentrated windings', IEEE Trans. Energy Convers., 2006, **21**, (1), pp. 34-43.
[11] El-Refaie A. M., 'Fractional-slot concentrated-windings synchronous permanent magnet machines: opportunities and challenges', IEEE Trans. Ind. Electron., 2010, **57**, (1), pp. 107-121.
[12] Spargo C. M., Mecrow B. C., Widmer J. D. , Morton C., 'Application of fractional-slot concentrated windings to synchronous reluctance motors', IEEE Trans. Ind. Appl., 2015, **51**, (2), pp. 1446-1455.
[13] Li G. J., Ma X. Y., Jewell G. W., Zhu Z. Q. , Xu P. L., 'Influence of conduction angles on single-layer switched reluctance machines', IEEE Trans. Magn., 2016, **52**, (12), pp. 1-11.
[14] Li G. J., Ojeda J., Hlioui S.*, et al.*, 'Modification in rotor pole geometry of mutually coupled switched reluctance machine for torque ripple mitigating', IEEE Trans. Magn., 2012, **48**, (6), pp. 2025-2034.
[15] Fiedler J. O., Kasper K. A. , Doncker R. W. D., 'Calculation of the acoustic noise spectrum of SRM using modal superposition', IEEE Trans. on Ind. Electron., 2010, **57**, (9), pp. 2939-2945.
[16] Zhu Z. Q., Liu X. , Pan Z., 'Analytical model for predicting maximum reduction levels of vibration and noise in switched reluctance machine by active vibration cancellation', IEEE Trans. Energy Convers., 2011, **26**, (1), pp. 36-45.
[17] Pellegrino G., Cupertino F. , Gerada C., 'Barriers shapes and minimum set of rotor parameters in the automated design of Synchronous Reluctance machines', Int. Conf. Electric Machines & Drives, 2013, pp. 1204-1210.
[18] Wang K., Zhu Z. Q., Ombach G.*, et al.*, 'Optimal slot/pole and flux-barrier layer number combinations for synchronous reluctance machines', Int. Conf. EVER, 2013, pp. 1-8.
[19] Kolehmainen J., 'Synchronous reluctance motor with form blocked rotor', IEEE Trans. Energy Convers., 2010, **25**, (2), pp. 450-456.
[20] Moghaddam R. R., Magnussen F. , Sadarangani C., 'Theoretical and experimental reevaluation of synchronous reluctance machine', IEEE Trans. Ind. Electron., 2010, **57**, (1), pp. 6-13.
[21] Vagati A., Pastorelli M., Francheschini G. , Petrache S. C., 'Design of low-torque-ripple synchronous reluctance motors', IEEE Trans. Ind. Appl., 1998, **34**, (4), pp. 758-765.
[22] Bianchi N., Mahmoud H. , Bolognani S., 'Fast synthesis of permanent magnet assisted synchronous reluctance motors', IET Elec. Power Appl., 2016, **10**, (5), pp. 312-318.
[23] Guan Y., Zhu Z. Q., Afinowi I. A. A., Mipo J. C. , Farah P., 'Design of synchronous reluctance and permanent magnet synchronous reluctance machines for electric vehicle application', ICEMS, 2014, pp. 1853-1859.
[24] Li G. J., Ojeda J., Hoang E., Lecrivain M. , Gabsi M., 'Comparative studies between classical and mutually coupled switched reluctance motors using thermal-electromagnetic analysis for driving cycles', IEEE Trans. Magn., 2011, **47**, (4), pp. 839-847.
[25] Zhu Z. Q., 'A simple method for measuring cogging torque in permanent magnet machines', IEEE Power & Energy Society General Meeting, 2009, pp. 1-4.